Int J Clin Exp Pathol 2026;19(8):370-384
www.ijcep.com /ISSN:1936-2625/IJCEP0171505

Original Article

Arterial origin-dependent susceptibility of vascular smooth muscle cells to prelamin A-induced senescence and rescue by umbilical artery-derived decellularized extracellular matrix

Kexin Guo[1,2], Qun Wan[3], Zhiwei Li[4], Xiaohua Xie[5], Yannv Qu[1,2]

[1]Geriatrics Department, Peking University Shenzhen Hospital, Shenzhen Peking University-The Hong Kong University of Science and Technology Medical Center, 1120 Lianhua Road, Futian District, Shenzhen 518036, Guangdong, China; [2]Medical School Department, Shenzhen University, 3688 Nanhai Road, Nanshan District, Shenzhen 518060, Guangdong, China; [3]Clinical Nutrition Department, Shenzhen University General Hospital, Shenzhen 518055, Guangdong, China; [4]Medical Records Department, The Chinese University of Hong Kong Shenzhen Medical Centre, 401 Jihua Road, Longgang District, Shenzhen 518172, Guangdong, China; [5]Chinese PLA General Hospital, 28 Fuxing Road, Haidian District, Beijing 100853, China

Received January 16, 2026; Accepted August 20, 2026; Epub August 25, 2026; Published August 30, 2026

Abstract: Objectives: To determine whether prelamin A (PLA) induces distinct senescence responses in vascular smooth muscle cells (VSMCs) from different arterial origins and whether the extracellular matrix (ECM) modulates these effects. Methods: PLA expression was examined in renal arteries from age-matched patients (59-63 years old). Human umbilical artery smooth muscle cells (huaSMCs) and human aortic smooth muscle cells (haoSMCs) were transduced with GFP- or PLA-expressing adenoviral vectors. Senescence, proliferation, DNA damage, apoptosis-related genes, ECM-related transcripts, and AKT/β-catenin signaling were assessed using X-GAL staining, Ki-67 staining, Cell Counting Kit-8 assays, γH2AX staining, quantitative PCR, and western blotting. HuaSMC-derived decellularized ECM (dECM) was applied to PLA-overexpressing haoSMCs. Results: PLA expression differed significantly among renal arteries from age-matched patients ($P < 0.005$). PLA overexpression induced nuclear abnormalities, increased γH2AX and X-GAL staining, and reduced Ki-67 expression in both huaSMCs and haoSMCs ($P < 0.001$). However, downstream responses differed between the two cell types. PLA-overexpressing huaSMCs showed increased p53 without significant p21 induction and reduced BCL-2, BAX, and CASP3 expression, whereas overexpressing haoSMCs exhibited increased p53, p21, BCL2, and CASP3 expression ($P < 0.05$ or $P < 0.001$). COL3A1 expression decreased only in PLA-overexpressing haoSMCs. HuaSMC-derived dECM reduced senescence-associated staining, improved proliferation, increased p-AKT, and reduced β-catenin signaling in PLA-overexpressing haoSMCs. Conclusions: PLA induces senescence-associated abnormalities in VSMCs from different arterial origins, but the downstream signaling and ECM responses differ markedly. HuaSMC-derived dECM partially attenuates PLA-induced dysfunction in aortic VSMCs, potentially through modulation of AKT/β-catenin signaling.

Keywords: Prelamin A, vascular smooth muscle cells, arterial origin, extracellular matrix, AKT signaling

Introduction

Vascular smooth muscle cell (VSMC) senescence is a significant contributor to age-related vascular dysfunction and atherosclerotic disease. Senescent VSMCs accumulate in aged vessels and atherosclerotic plaques and exhibit persistent DNA damage response (DDR) activation and a senescence-associated secretory phenotype (SASP), thereby promoting inflammation and maladaptive vascular remodeling [1-3]. Telomere dysfunction and chronic DNA damage are key triggers of VSMC senescence [4, 5].

Prelamin A (PLA), the immature precursor of lamin A, accumulates in aging VSMCs and acts as both a biomarker and driver of vascular aging. PLA induces nuclear morphological abnormalities, persistent DDR signaling, impaired

https://doi.org/10.62347/BIWL1982

mitosis, and accelerated senescence in VSMCs [1, 2]. Furthermore, DDR-mediated and SASP-related mechanisms are implicated in vascular calcification [2]. Both classical and more recent studies have identified PLA as a mechanistic link between nuclear lamina defects and VSMC aging [1, 2, 6].

Although PLA accumulation is a potent pro-senescence stressor in VSMCs, cellular responses may not be uniform across the vasculature. VSMCs exhibit considerable phenotypic, transcriptional, and functional heterogeneity determined by embryologic lineage, anatomical location, and local mechanical and biochemical cues. These factors may influence how VSMCs engage DDRs, p53/p21 signaling, and apoptotic programs during aging and diseases [1, 2, 6, 7]. Single-cell and lineage-tracing studies have demonstrated vessel-bed-specific VSMC states and disease-relevant transcriptional signatures, further indicating that VSMC origin can influence downstream phenotypic outcomes [8]. Whether VSMCs from distinct arterial origins, such as umbilical artery and aorta, activate divergent signaling and functional programs in response to the same senescence-inducing stimulus therefore remains an important question [7, 9].

The extracellular matrix (ECM) is a dynamic and instructive microenvironment that regulates VSMC phenotype, proliferation, migration, and survival. ECM composition and organization change substantially with aging and vascular disease, thereby modulating intracellular pathways, including phosphoinositide 3-kinase (PI3K)-protein kinase B (AKT) and Wnt/β-catenin signaling [10-13]. Recent reviews and transcriptomic/proteomic studies have emphasized that ECM-receptor interactions and ECM remodeling are closely associated with VSMC functional states and vascular remodeling in disease [11, 12]. Decellularized ECM (dECM), particularly cell-derived dECM that preserves tissue-specific matricellular cues, can restore niche signals and modulate cell behavior in vitro, supporting its experimental use to promote survival, proliferation, and phenotypic normalization in diverse cell types [14, 15]. Thus, ECM composition may influence VSMC responses to PLA and provide a potential approach for attenuating deleterious PLA-induced phenotypes.

In this study, we tested the hypothesis that arterial origin influences VSMC responses to PLA and investigated whether tissue-specific ECM mitigate PLA-induced dysfunction. We compared the effects of PLA overexpression in human umbilical artery smooth muscle cells (huaSMCs) and human aortic smooth muscle cells (haoSMCs). Specifically, we aimed to (1) characterize arterial origin-dependent senescence, DNA damage, and apoptosis-related responses to PLA; (2) quantify changes in ECM-related gene expression following PLA overexpression; and (3) determine whether huaSMC-derived dECM attenuates PLA-associated phenotypes in haoSMCs, with a focus on AKT and β-catenin signaling.

Materials and methods

Human tissue specimens and immunohistochemistry

Formalin-fixed, paraffin-embedded renal artery specimens were obtained from six patients aged 59-63 years who underwent nephrectomy for nonvascular indications, including hydronephrosis with renal atrophy and renal clear cell carcinoma. All samples were obtained with the approval of the Institutional Review Board of the Peking University Shenzhen Hospital Clinical Research Center Ethics Committee. Written informed consent was obtained from all patients in accordance with the Declaration of Helsinki.

Formalin-fixed, paraffin-embedded blocks were sectioned at a thickness of 4 μm, deparaffinized, and subjected to heat-induced antigen retrieval in citrate buffer (pH 6.0). Endogenous peroxidase activity was quenched with 3% H_2O_2. Sections were incubated overnight with an anti-PLA primary antibody (mouse monoclonal; sc-518013 C-3; Santa Cruz Biotechnology) at a dilution of 1:200, followed by incubation with a horseradish peroxidase-conjugated secondary antibody and detection with diaminobenzidine (DAB). Hematoxylin was used as a counterstain. Negative controls were processed identically, except for omission of the primary antibody.

Staining intensity and the percentage of positively stained VSMCs were independently evaluated by two blinded pathologists. Digital IHC images were also analyzed using ImageJ soft-

ware. Color deconvolution was applied to separate the DAB and hematoxylin channels, and the DAB-positive area was quantified using a fixed threshold. The positive area fraction was calculated as the ratio of DAB-positive pixels to the total vessel wall area. Measurements were performed in at least three randomly selected fields per specimen.

Cell culture

HuaSMCs were obtained from Professor Zhang Weiyi (Department of Obstetrics and Gynecology, Peking University Shenzhen Hospital). Primary huaSMCs were isolated from fresh human umbilical cord samples obtained from healthy donors with written informed consent. Cells were maintained in Dulbecco's modified Eagle's medium/F12 supplemented with 10% fetal bovine serum and 1% penicillin-streptomycin at 37°C in a 5% CO_2 atmosphere. Cells at passages 3-8 were used in this study. Primary haoSMCs (CC-2571; LONZA) were cultured in SmGM-2 Smooth Muscle Cell Growth Medium-2 (CC-3182; LONZA). Cells at passages 3-8 were used in all experiments. Both cell types were validated by morphological analysis and α-smooth muscle actin expression and were confirmed to be negative for Mycoplasma. HuaSMCs and haoSMCs were used for all in vitro experiments.

PLA overexpression

Replication-deficient adenoviruses encoding human PLA (pHS-AVC-LW1016) or a green fluorescent protein (GFP) control were generated in AD293 cells using a commercial packaging kit (Beijing Syngentech Co., Ltd.) [16]. HuaSMCs and haoSMCs were transduced at a multiplicity of infection of 30-50. Transduction efficiency was confirmed by GFP expression (> 80%) and PLA detection by western blotting. Unless otherwise specified, assays, including SA-β-gal staining, Ki-67 immunostaining, and western blottin, were performed 48 h after adenoviral infection.

To distinguish cell origin and viral treatment, the following nomenclature was used throughout the study: GFP-ua and PLA-ua refer to GFP- and PLA-transduced huaSMCs, respectively, whereas GFP-ao and PLA-ao refer to GFP- and PLA-transduced haoSMCs, respectively.

Senescence, proliferation, and cell death assays

SA-β-galactosidase quantification: Senescence was assessed using a commercial Senescence β-Galactosidase Staining Kit (#9860S; Cell Signalling Technology) at pH 6.0, according to the manufacturer's protocol. SA-β-gal-positive cells were counted in at least five randomly selected fields per sample. X-GAL staining was further quantified using ImageJ software [17]. Bright-field images were converted to 8-bit grayscale images and threshold to isolate X-GAL-positive areas. The percentage of the positive area was calculated by dividing the X-GAL-stained area by the total cell-covered area. At least five randomly selected fields were analyzed for each sample.

Cell Proliferation was measured at 0, 24, and 72 h post-infection using a (Cell Counting Kit [CCK]-8) according to the manufacturer's instructions. Cells were seeded in 96-well plates at a density of 5×10^3 cells/well. Absorbance was measured at 450 nm, and each experiment was performed in triplicate.

Annexin V/7-amino-actinomycin D (7-AAD) staining: For cell death analysis, cells were harvested 48 h post - infection by trypsinization, washed twice with cold PBS, and resuspended in Annexin V Binding Buffer (BioLegend) at a concentration of 1×10^6 cells/mL. A 100 μL aliquot of the cell suspension (1×10^5 cells) was transferred to a 5 mL tube and stained with 5 μL of 7-AAD (BioLegend, #640930) for 15 min at room temperature in the dark. After staining, 400 μL of Annexin V Binding Buffer was added, and samples were immediately analyzed using a BD FACSCanto II flow cytometer. At least 10,000 events were acquired per sample. The percentage of 7-AAD-positive cells was quantified using FlowJo software (v10.10.1).

Immunofluorescence assay and nuclear morphology assessment

Smooth muscle cells were fixed with 4% paraformaldehyde, permeabilized with 0.5% Triton X-100, and incubated overnight at 4°C with primary antibodies against γH2AX (Ser139; 1:400; #2577; CST) and Ki-67 (1:200; #ab-15580; Abcam). After washing, cells were incubated with species-matched goat anti-rabbit IgG secondary antibody (Alexa Fluor® 594,

Table 1. Gene-specifc reference primer sequences utilized for qRT-PCR analysis

Primer	Sequences (5' to 3')
H-COL3A1-F	tgc tgc tgg tac tcc tgg tct g
H-COL3A1-R	acc tgg acc gcc tgg ttc ac
H-COL1A1-F	aaa gat gga ctc aac ggt ctc
H-COL1A1-R	cat cgt gag cct tct ctt gag
H-Bcl2-F	gac ttc gcc gag atg tcc ag
H-Bcl2-R	gaa ctc aaa gaa ggc cac aat c
H-CASP3-F	cca aag atc ata cat gga agc g
H-CASP3-R	ctg aat gtt tcc ctg agg ttt g
H-Bax-F	cga act gga cag taa cat gga g
H-Bax-R	cag ttt gct ggc aaa gta gaa a

1:500, #ab150080; Abcam) at room temperature for 1 h, followed by nuclear counterstaining with DAPI (1:25,000, #zli-9557; Zhongshan Golden Bridge Biotechnology). Then, nuclear morphology in approximately 100 randomly selected cells per condition was rigorously evaluated. Abnormal nuclei, defined by the presence of blebbing, lobulation, or micronucleation, were quantified as a percentage of the total nuclei scored.

For immunofluorescence analysis of ECM components, dECM samples were fixed with 4% paraformaldehyde and incubated overnight at 4°C with primary antibodies against collagen type III (COL3; N-terminal; 1:50; #22734-1-AP; Proteintech), and fibronectin (1:50; #66042-1-Ig; Proteintech). After washing, samples were incubated with species-matched secondary antibodies - goat anti-rabbit IgG (for COL3; Alexa Fluor® 594, 1:500, #ab150080; Abcam) and goat anti-mouse IgG (for fibronectin; Alexa Fluor® 647, 1:500, #ab150115; Abcam) - at room temperature for 1 h. Nuclei were counterstained with DAPI (1:25,000, #zli-9557; Zhongshan Golden Bridge Biotechnology). Samples were mounted with antifade mounting medium and visualized using a confocal laser scanning microscope. Images were acquired using identical acquisition parameters across all experimental groups. Fluorescence intensity was quantified using the ImageJ software with uniform background subtraction.

Western blotting analysis

Smooth muscle cells were lysed using radioimmunoprecipitation assay buffer containing protease and phosphatase inhibitors. Protein concentrations were measured via bicinchoninic acid assay. Equal amounts of protein (20-30 μg) were resolved via sodium dodecyl sulfate-polyacrylamide gel electrophoresis and transferred to polyvinylidene fluoride membranes. After blocking, the membranes were incubated overnight at 4°C with primary antibodies against PLA (sc-518013 C-3; Santa Cruz), lamin A/C (sc-6215; Santa Cruz), p53 (#2524; CST), p21 (#2947; CST), p16 (#80772; CST), collagen type III (#22734-1-AP; Proteintech), fibronectin (#66042-1-Ig; Proteintech), phospho-AKT (Ser473; #4060; CST), total AKT (#4691; CST), phospho-β-catenin (Ser33/37/Thr41; #9561; CST), total β-catenin (#8480; CST), and γH2AX (#2577; CST), with glyceraldehyde-3-phosphate dehydrogenase (GAPDH; #2118; CST) and β-actin (sc-47778; Santa Cruz) as loading controls.

Primary antibodies were used at a dilution of 1:1000. Horseradish peroxidase-conjugated secondary antibodies were subsequently applied, and protein bands were visualized via enhanced chemiluminescence assay. The protein sample loading volume was 20 μL/well. Regarding the loading controls, using two distinct controls without establishing a unified standard gives rise to unnecessary variability. GAPDH and β-actin were used at a dilution of 1:1000. Densitometric analysis was performed using the gel analysis tool in ImageJ with uniform background correction. Protein expression levels were normalized to GAPDH or β-actin. Data represent the mean values of at least three independent experiments.

Quantitative polymerase chain reaction (qPCR)

Real-time qPCR was performed using the FTC-3000P Real-Time PCR System. All primer sequences for the target genes are listed in **Table 1**. Reaction were performed using the SYBR Premix Ex Taq kit (Cat# RR420A; Takara) according to the manufacturer's instructions. Each reaction was performed in a total volume of 20 μL, containing 2 μL of cDNA and 0.4 μM of each primer. The thermal cycling conditions were as follows: initial denaturation at 95°C for 3 min, followed by 40 cycles of denaturation at 95°C for 15 s, annealing at 60°C for 15 s, and extension at 72°C for 15 s. Melting curve analysis was performed at the end of the cycling pro-

gram to verify amplification specificity. Relative gene expression levels were normalized to *GAPDH* and calculated using the $2^{-\Delta\Delta Ct}$ method.

dECM preparation

dECM was prepared as previously described [18], with some modifications. Briefly, confluent huaSMC monolayers were cultured for 10 days to allow ECM deposition. The culture medium was aspirated, and cells were washed three times with ice-cold sterile phosphate-buffered saline. Sterile deionized water was then added, and the cells were incubated at room temperature for 5 min. After removal of the deionized water, 0.5% (v/v) Triton X-100 (×100; Sigma-Aldrich) was added, and the cells were incubated at room temperature for 5-10 min. Nuclear detachment was monitored microscopically, and the reaction was terminated by replacing the solution with phosphate-buffered saline once most nuclei had disappeared. Decellularization was confirmed by the absence of nuclei on DAPI staining. The dECM sheets were stored at 4°C for short-term use or at -80°C for long-term storage.

Seeding experiments on huaSMC-derived dECM

PLA-overexpressing haoSMCs (PLA-ao) were harvested and seeded on huaSMC-derived dECM-coated coverslips or culture plates (PLA-ao + ECM) at a density of 2×10^4 cells/cm^2. PLA-ao cells cultured on plastic were used as controls. Cultures were maintained for 7 days, with the medium replaced every two days.

Statistical analyses

All experiments were performed with at least three biological replicates. Data are presented as mean ± standard deviation. Statistical analyses were performed using GraphPad Prism version 8.3.0 software (GraphPad Software, San Diego, CA, USA). For comparisons between GFP- and PLA-transduced cells within each cell type (GFP-ua vs. PLA-ua or GFP-ao vs. PLA-ao), two-tailed unpaired Student's t-tests were used. These comparisons included SA-β-gal staining, Ki-67 and γH2AX immunofluorescence, CCK-8 assays, western blot densitometry, and qPCR analysis. For experiments involving more than two groups, including comparisons among GFP-ao, PLA-ao, and PLA-ao + ECM groups, one-way analysis of variance, followed by Tukey's post-hoc test was used. Normality was assessed before parametric testing, and appropriate nonparametric tests were used when the data were not normally distributed. A two-sided $P < 0.05$ was considered statistical significant.

Results

PLA levels vary among the renal arteries of age-matched patients

Immunohistochemical staining was performed on renal artery specimens from six age-matched patients (59-63 years old) who underwent nephrectomy for nonvascular renal conditions (hydronephrosis with renal atrophy, n = 3; renal clear cell carcinoma, n = 3). As shown in **Figure 1A-C** (a 63-year-old male with renal clear cell carcinoma) and **Figure 1D-F** (a 59-year-old male with hydronephrosis and renal atrophy), PLA expression exhibited marked interindividual heterogeneity despite the similar chronological ages of the patients ($P < 0.005$; **Figure 1G**). Semi-quantitative analysis showed no statistically significant difference in the PLA-positive staining area between the two patient groups ($P > 0.05$; **Figure 1H**).

PLA overexpression induces senescence and DNA damage in VSMCs with arterial origin-dependent molecular responses

PLA-expressing umbilical artery and aortic SMCs are referred to as PLA-ua and PLA-ao cells, respectively, with their corresponding GFP controls designated as GFP-ua and GFP-ao cells.

PLA-ua and PLA-ao cells exhibited prominent PLA accumulation at the nuclear envelope and abnormal nuclear morphology, including nuclear blebs and lobulations (**Figure 2A-D**). PLA overexpression was confirmed by western blotting ($P < 0.0001$; **Figure 2E-H**).

Senescence-associated β-galactosidase staining showed that PLA overexpression significantly increased the X-GAL-positive area in both PLA-ua and PLA-ao cells ($P < 0.001$; **Figure 3A-F**). Ki-67 immunostaining showed reduced proliferation following PLA overexpression (**Figure 3G-J**), whereas γH2AX staining intensity was markedly increased in both cell types, indi-

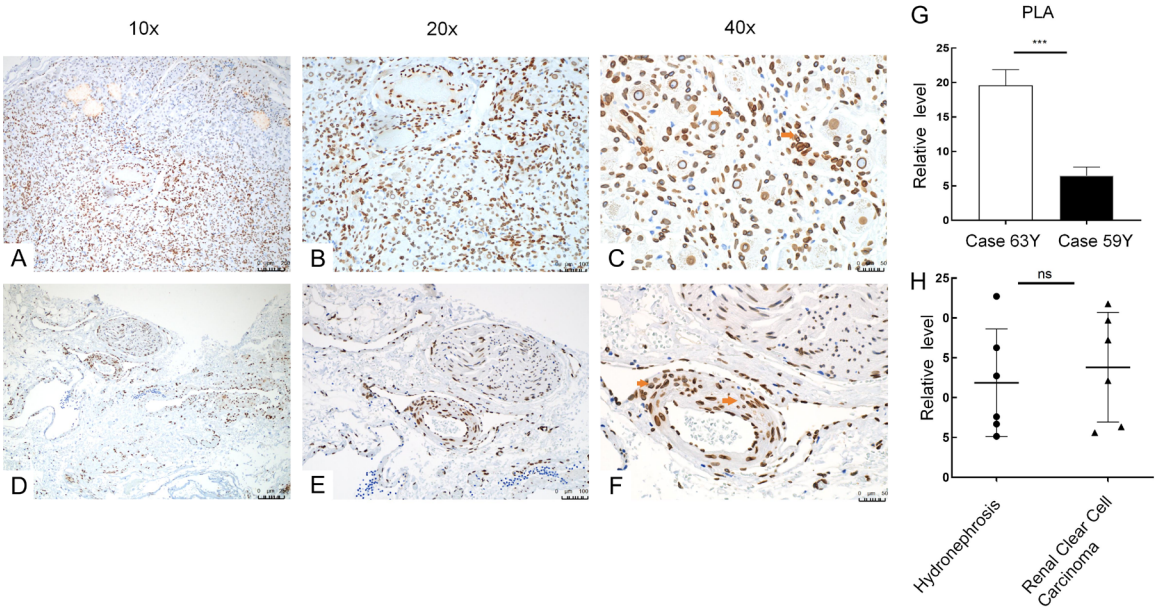

Figure 1. Prelamin A expression in renal artery tissues. (A-F) Representative IHC images showing PLA staining in renal arteries from renal tissue from a 63-year-old male with renal clear cell carcinoma (A-C) and renal tissue from a 59-year-old male with hydronephrosis and renal atrophy (D-F). (G) Quantification of PLA-positive area. (H) PLA between specimens from the two patient groups. The arrows indicate the positively stained cells. ***P < 0.005. Scale bar = 50-250 μm. Abbreviation: PLA, prelamin A.

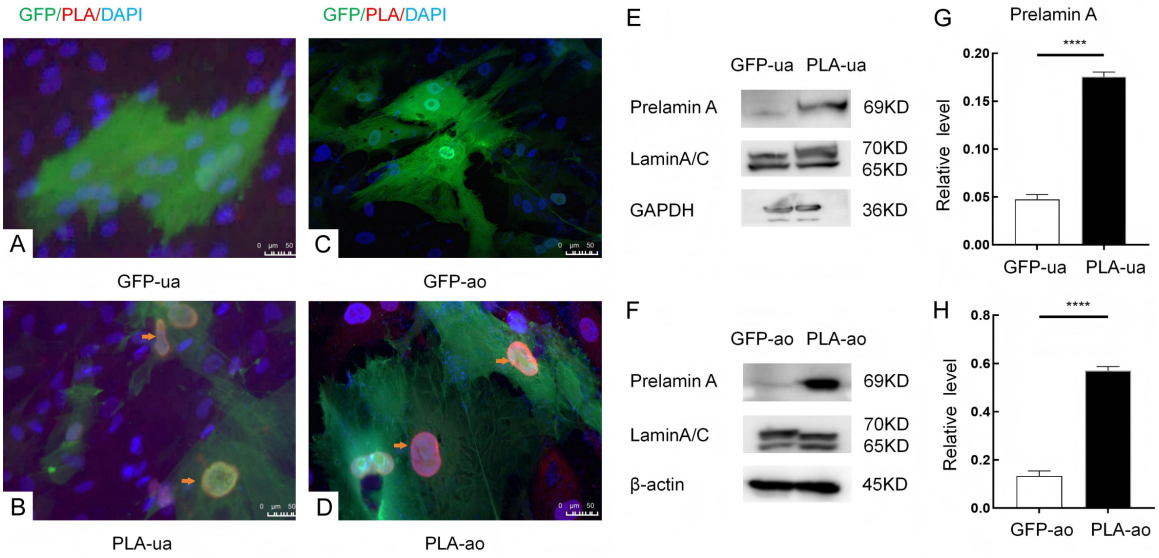

Figure 2. PLA-ua and PLA-ao exhibit nuclear abnormalities. A-D. Nuclear envelope accumulation of PLA and irregular nuclear morphology (blebs, lobulations) in PLA-ua and PLA-ao cells. E, F. Western blot confirmation of PLA overexpression. Scale bar = 100 μm. G, H. Quantification of Prelamin A protein expression, ****P < 0.0001, PLA vs. GFP control.

cating increased DNA damage. Western blotting further confirmed the increase in γH2AX (P < 0.0001; **Figure 3K-R**).

Although PLA induced senescence-associated changes in both cell types, their downstream molecular responses differed. In PLA-ua cells, p53 levels increased without a significant change in p21, whereas both p53 and p21 levels increased in PLA-ao cells (**Figure 4A**; densitometric quantification shown in **Figure 4B**). qRT-PCR further demonstrated decreased

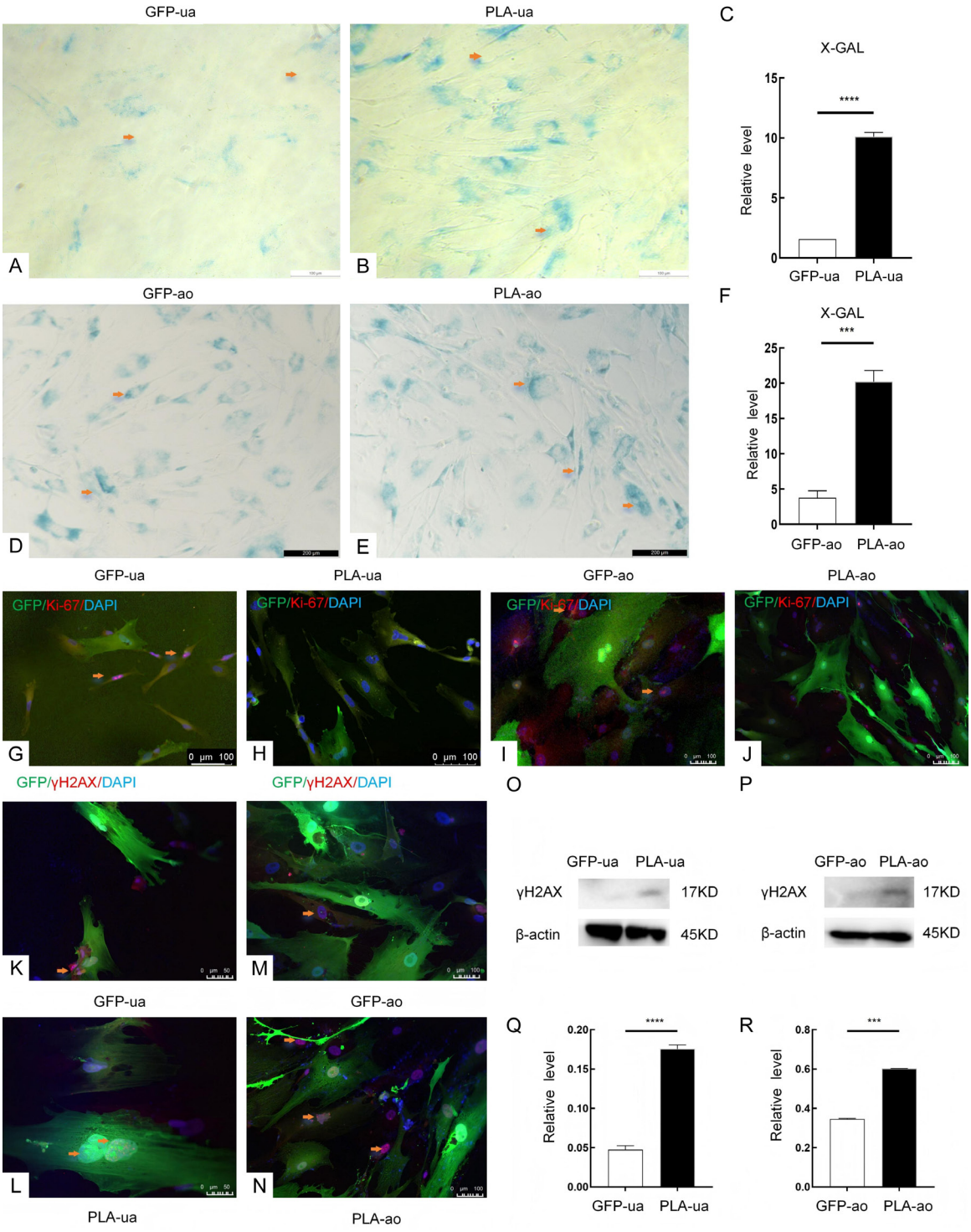

Figure 3. PLA induces senescence, reduces proliferation, and causes DNA damage. PLA induces senescence, reduces proliferation, and causes DNA damage. (A-F) SA-β-gal staining showing increased senescence in PLA-ua and PLA-ao cells. Arrows indicate positively stained cells. (G-J) Immunofluorescence staining showing reduced Ki-67 and increased γH2AX foci (K-N) in PLA-overexpressing cells. (O, P) Quantification of γH2AX positive cells. (Q, R) Western blot analysis of γH2AX expression. Data are presented as mean ± SD. ***P < 0.005, ****P < 0.0001, PLA vs. GFP control. Scale bar = 100 μm. Abbreviation: X-GAL, SA-β-gal-positive staining.

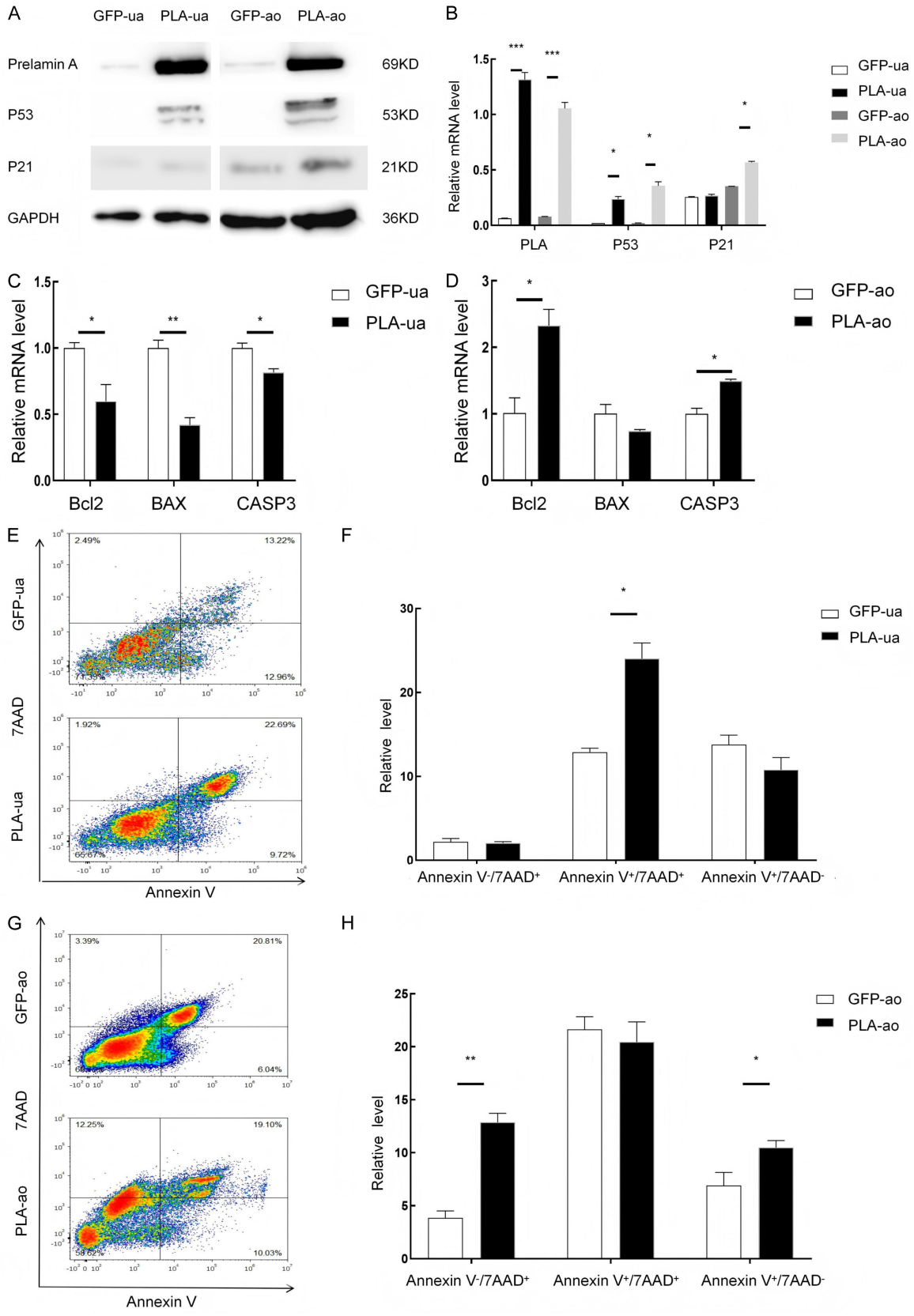

Figure 4. Divergent p53/p21 and apoptosis-related gene expression in PLA-ua vs. PLA-ao. (A) Western blot analysis showing increased p53 in PLA-ua and increased p53/p21 in PLA-ao. (B) Densitometric quantification of p53 and

p21. (C, D) qRT-PCR analysis of BCL2, BAX, and CASP3 expression in GFP-ua, PLA-ua, GFP-ao, and PLA-ao (*P < 0.05, **P < 0.01, ***P < 0.005), PLA vs. GFP control. Flow cytometric analysis of Annexin V/7AAD staining in (E, F) GFP-ua vs. PLA-ua and (G, H) GFP-ao vs. PLA-ao. Quantification represents mean ± SEM from n = 3 independent experiments analyzed separately within each VSMC type. Statistical significance determined by unpaired two-tailed Student's t-test: *P < 0.05, **P < 0.01. No cross-type statistical comparison was performed as the primary objective was to assess PLA effects within each VSMC lineage independently. Abbreviation: PLA, prelamin A.

BCL2, BCL-2-associated X, and caspase (*CASP*)-*3* expression in PLA-ua cells, whereas *BCL2* and *CASP3* expression increased in PLA-ao cells (**Figure 4C**, **4D**). Flow cytometric analysis further demonstrated distinct cell death profiles following PLA overexpression in the two cell types (**Figure 4E-H**).

PLA differentially alters ECM-related gene expression in artery-derived VSMCs

We previously investigated PLA-induced gene expression changes during mesenchymal stem cell senescence [16]. KEGG enrichment analysis of the mesenchymal stem cell-derived dataset identified ECM-receptor interaction (P = 0.0018), glycosphingolipid biosynthesis (P = 0.002), and protein digestion and absorption (P = 0.0035) among the most significantly enriched pathways; the PI3K-Akt signaling pathway was also significantly enriched (P = 0.0086; **Figure 5A**). Targeted qRT-PCR validation showed that COL3A1 expression was significantly lower in PLA-ao cells than in GFP-ao cells (P < 0.01), whereas no significant difference was observed between PLA-ua and GFP-ua cells. In contrast, COL1A1 expression remained unchanged in both cell types (**Figure 5B-E**).

Umbilical artery-derived dECM attenuates PLA-induced dysfunction in haoSMCs

The preparation of huaSMC-derived dECM is shown in **Figure 6A-C**. DAPI staining (**Figure 6D**, **6E**) confirmed the removal of residual cellular nuclei following decellularization. Immunofluorescence staining confirmed the presence of key ECM components, including collagen III and fibronectin, in the dECM (**Figure 6F**, **6G**). Western blotting further confirmed the presence of these proteins in the dECM preparations (**Figure 6H**, **6I**).

PLA-ao cells cultured on dECM (PLA-ao + ECM) exhibited a marked reduction in the X-GAL-positive area compared with PLA-ao cells cultured on standard plastic (**Figure 6J-M**). Ki-67 immunofluorescence showed increased proliferation in PLA-ao + ECM compared with PLA-ao cells cultured without dECM (**Figure 6N-P**), and CCK-8 assays further confirmed enhanced proliferation in the dECM-treated group (P < 0.05; **Figure 6Q**).

Western blotting showed that dECM treatment increased p-AKT levels in PLA-ao cells without altering total AKT levels. In contrast, β-catenin and p-β-catenin levels, which were elevated in PLA-ao cells, were reduced following culture on dECM (**Figure 6R**; densitometric quantification shown in **Figure 6S**).

Discussion

This study delineated the effects of pathological PLA accumulation in VSMCs from two distinct arterial origins: the human umbilical artery and aorta. PLA induced core features of cellular senescence, including nuclear envelope abnormalities, DNA damage, and reduced proliferation, in both cell types. However, downstream signaling responses and ECM responses differed substantially between umbilical and aortic VSMCs. Notably, dECM derived from umbilical artery VSMCs partially restored the proliferative capacity of PLA-expressing aortic VSMCs and modulated AKT/β-catenin signaling. These findings highlight arterial origin-dependent heterogeneity in VSMC responses to PLA and suggest that matrix-derived cues may modulate cellular responses to nuclear envelope stress.

VSMCs are not a homogeneous cell population but retain origin-specific identities with functional consequences. Developmental lineage studies and single-cell atlases have demonstrated that VSMCs across the vascular tree differ in embryologic origin, gene expression programs, and capacity for phenotypic modulation [7, 8, 19]. Mühl et al. identified distinct vascular and visceral SMC states and vessel-specific ECM and signaling signatures, indicating that regional identity is encoded at both transcriptional and protein levels [8]. Structurally, elastic arteries such as the aorta differ from

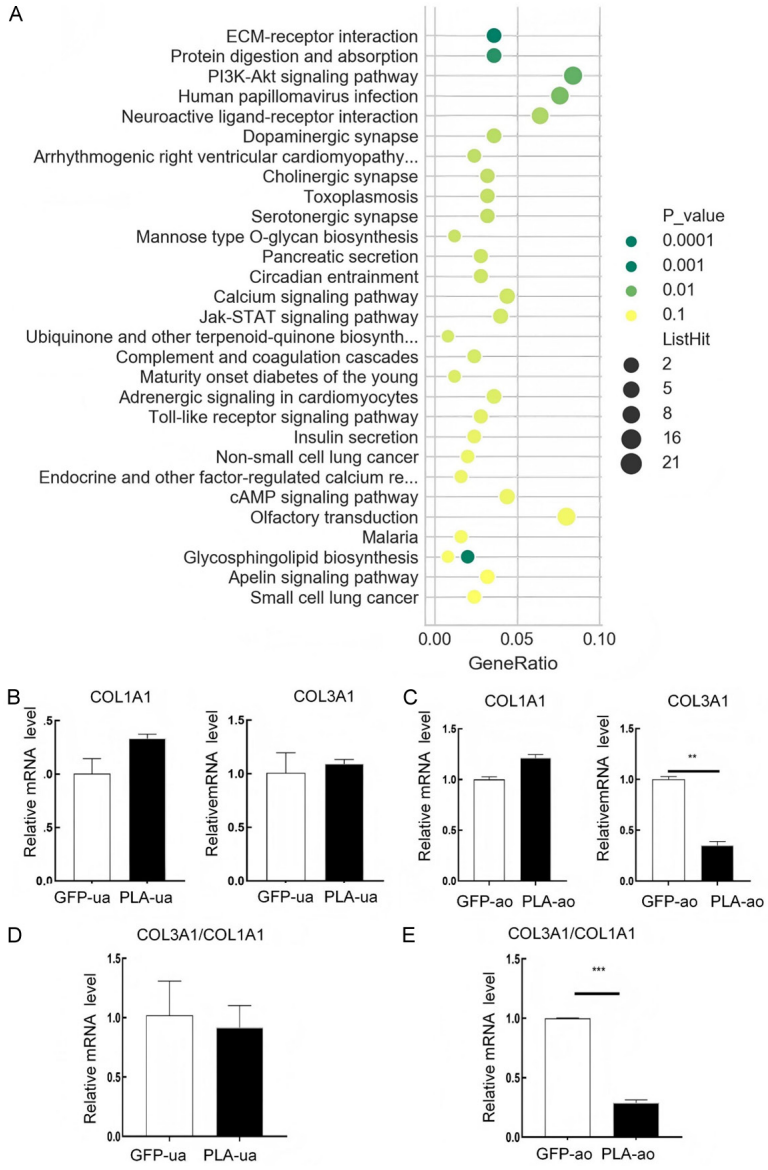

Figure 5. Differential ECM gene expression following PLA overexpression. A. KEGG enrichment of gene expression profiles in mesenchymal stem cells. B, C. qRT-PCR analysis of COL1A1 and COL3A1 expression in GFP-ua, PLA-ua, GFP-ao, and PLA-ao. D, E. qRT-PCR analysis of COL3A1/COL1A1 expression in different groups (**P < 0.01, ***P < 0.005), PLA vs. GFP control. Abbreviation: ECM, extracellular matrix.

muscular or umbilical arteries in wall architecture and ECM composition, including collagen I/III, elastin, and proteoglycans, resulting in distinct mechanotransductive signaling and basal transforming growth factor (TGF)-β activity [1-3]. Such differences may influence how nuclear envelope perturbation caused by PLA accumulation is sensed and propagated. In our study, the selective reduction of COL3A1 expression in PLA-overexpressing aortic VSMCs further suggests that ECM responses to PLA differ according to arterial origin.

In addition to inducing structural abnormalities, pathological PLA accumulation disrupts chromatin anchoring to the nuclear lamina, potentially altering chromatin accessibility and the regulation of stress-responsive genes [20]. Nuclear lamina defects can also promote reorganization of lamina-associated domains, potentially affecting the spatial positioning and transcriptional regulation of p53- and p21-related loci [21]. These chromatin changes may influence whether VSMCs undergo cell-cycle arrest, senescence, or apoptosis, depending on the local chromatin environment and histone modification patterns [22]. Thus differences in cellular context between arterial origins may contribute to the distinct p53/p21 responses observed following PLA overexpression.

Aortic VSMCs may be particularly responsive to TGF-β-p21-dependent senescence signaling. In Marfan syndrome aortas, TGF-β1 activation through reactive oxygen species/nuclear factor-κB signaling increases p53 and p21 expression, an effect inhibited by mitochondrial antioxidants [23]. Similarly, angiotensin II-induced VSMC senescence involes TGF-β1/p38 mitogen-activated protein kinase-mediated p21 upregulation [24]. Integrin signaling may further reinforce response, as integrin αvβ3 can amplify TGF-β signaling through SASP-associated feedback [25]. Zhu et al. further demonstrated that aged rat VSMCs exhibit increased stiffness and frictional moduli associated with TGFβ1-mediated clustering of mechanosensitive integrins α5β1 and αvβ3

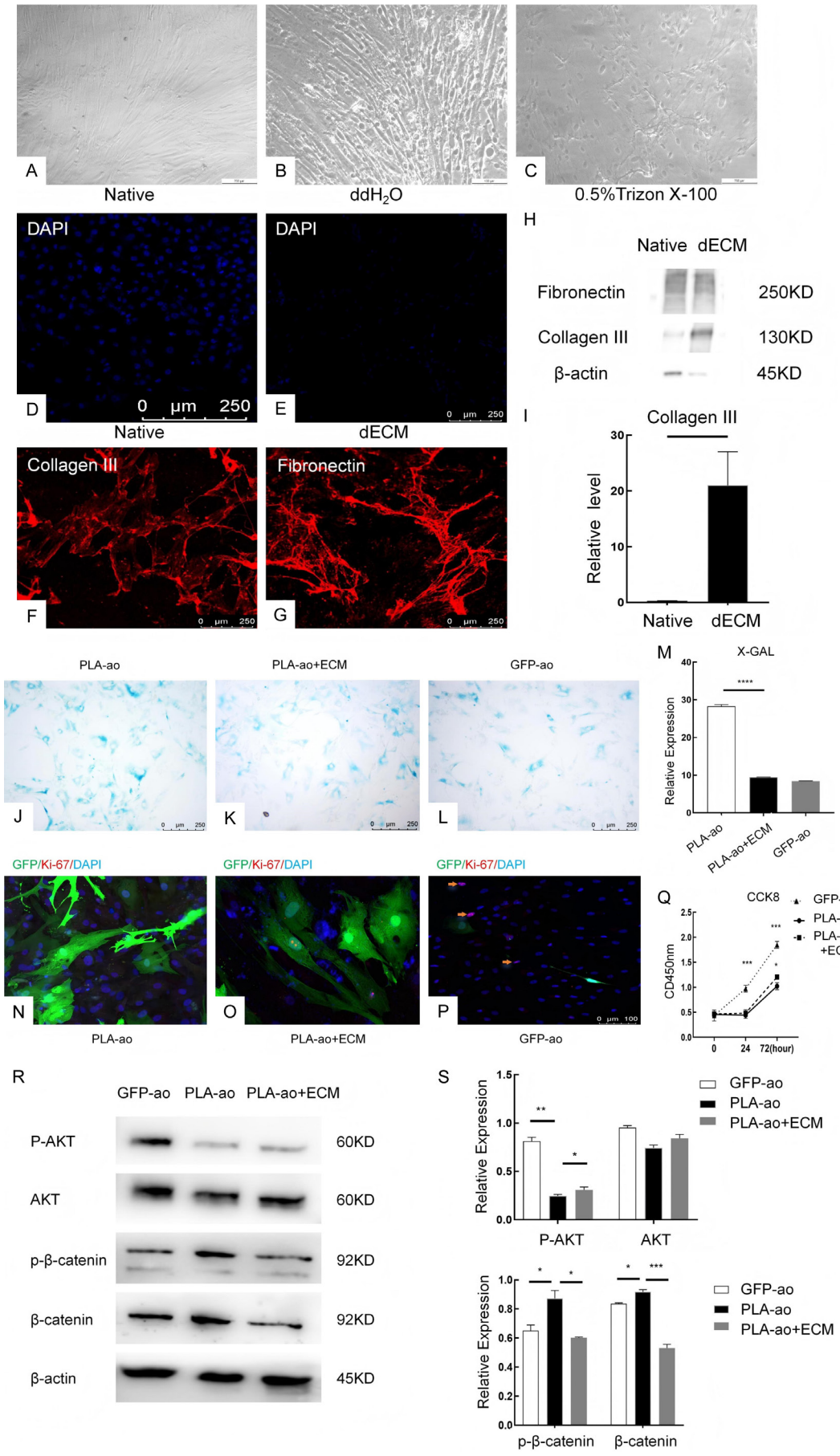
A
Native
B
ddH2O
C
0.5%Trizon X-100
DAPI
D
0 μm 250
Native
DAPI
E
dECM
H
Native dECM
Fibronectin
250KD
Collagen III
130KD
β-actin
45KD
Collagen III
F
Fibronectin
G
I
Collagen III
Relative level
Native dECM
PLA-ao
PLA-ao+ECM
GFP-ao
J
K
L
M
X-GAL
Relative Expression
PLA-ao
PLA-ao+ECM
GFP-ao
GFP/Ki-67/DAPI
N
O
P
PLA-ao
PLA-ao+ECM
GFP-ao
Q
CCK8
GFP-ao
PLA-ao
PLA-ao +ECM
CD450nm
0 24 72(hour)
R
GFP-ao PLA-ao PLA-ao+ECM
P-AKT
60KD
AKT
60KD
p-β-catenin
92KD
β-catenin
92KD
β-actin
45KD
S
Relative Expression
GFP-ao
PLA-ao
PLA-ao+ECM
P-AKT
AKT
p-β-catenin
β-catenin

Figure 6. Effects of huaSMC-derived decellularized ECM on PLA-ao cells. (A-C) The preparation of dECM. DAPI staining (D, E) confirmed the removal of residual cellular DNA following decellularization. (F, G) Immunofluorescence showing collagen III and fibronectin deposition within huaSMC-derived dECM. (H) Western blot analysizes the presence of the proteins in the dECM preparations. (I) Quantification of collagen III protein expression, **P < 0.001. (J-L) Representative X-GAL staining images of PLA-ao cells cultured on standard plastic or huaSMC-derived dECM, ***P < 0.005. (M) Quantification of X-GAL-positive area demonstrating reduced senescence in PLA-ao + ECM compared with PLA-ao. (N-P) Ki-67 immunofluorescence showing increased proliferative activity in PLA-ao + ECM. (Q) CCK-8 assay indicating enhanced cell proliferation in PLA-ao + ECM (*P < 0.01; ***P < 0.001). (R) Western blot analysis of p-AKT, total AKT, β-catenin, and phospho-β-catenin in GFP-ao, PLA-ao, and PLA-ao + ECM groups. (S) Densitometric quantification of protein expression normalized to loading controls. Scale bar = 100-250 μm. Abbreviations: ECM, extracellular matrix; dECM, decellularized extracellular matrix; CCK8, cell counting kit-8 assays.

[26]. Together, these studies support a close relationship among TGF-β signaling, mechanotransduction, and age-associated aortic VSMC dysfunction.

Consistent with this framework, PLA-overexpressing aortic VSMCs showed pronounced p21 induction together with altered expression of apoptosis-related genes, including *BCL2* and *CASP3*. Aortic VSMCs have also been reported to exhibit enhanced p53 acetylation, reinforcing the canonical p53-p21 signaling axis [27]. Although TGF-β or integrin activity was not directly measured in the present study, these pathways provide a plausible context for the strong p21 response observed in PLA-overexpressing aortic VSMCs. PLA-induced nuclear stress may therefore interact with pre-existing vessel-specific signaling programs to determine the cellular response.

huaSMCs (PLA-ua) exhibited a distinct response to PLA overexpression. Despite comparable nuclear envelope abnormalities and DNA damage, as indicated by γH2AX levels, PLA-ua cells did not induce p21 expression. Instead, they showed reduced expression levels of proapoptotic genes, including BCL-2-associated X and *CASP3*, while maintaining elevated *p53* levels. This divergence highlights the vessel-specific nature of PLA toxicity. It suggests that the aortic microenvironment, through its unique ECM composition, baseline TGF-β signaling, or chromatin architecture, primes cells for p21-dependent senescence. In contrast, the umbilical artery, which shows a distinct developmental origin and is exposed to different hemodynamic forces, may lack these priming cues. Consequently, it exhibits a blunted senescence response and alternative cell fate decisions.

Indeed, p53 signaling is highly context-dependent. In adipocytes, p53 can activate AMP-activated protein kinase-α and inhibit mechanistic target of rapamycin signaling, promoting reversible quiescence rather than permanent senescence [28]. Altered p53 phosphorylation can also redirect its transcriptional activity [29], while urocortin signaling suppresses TGF-β-induced p21 upregulation through cPLA2 inhibition [30]. In contrast, enhanced p53 acetylation in aortic VSMCs favors the canonical p53-p21 axis [27]. These These observations support the possibility that arterial identity influences the downstream consequences of PLA-induced p53 activation.

Additional regulators may contribute to this divergence. NORE1A-homeodomain-interacting protein kinase 2 complexes have been implicated in directing context-dependent p53 responses. High NORE1A expression can favor non-canonical p53 outputs under conditions associated with altered AMP-activated protein kinase and PI3K/Akt signaling [31], whereas homeodomain-interacting protein kinase 2 can promote p53 phosphorylation and p21 transcription [32]. Although these mechanisms were not directly examined in our study, they provide potential explanations for the divergent p53/p21 responses and warrant further investigation.

ECM-receptor interactions are increasingly recognized as important regulators of vascular aging and diseases [10, 33]. Cai et al. identified PI3K-AKT and Wnt/β-catenin signaling as important downstream effectors of ECM-mediated vascular remodeling [33], while Barallobre-Barreiro et al. demonstrated that changes in ECM composition are closely associated with vascular pathology and cellular phenotype [10]. In the present study, huaSMC-derived dECM attenuated senescence-associated phenotypes and improved proliferation in PLA-overexpressing aortic VSMCs. These effects suggest that the ECM acts not only as a structural scaffold but also as a signaling

microenvironment capable of modifying cellular responses to PLA-induced stress.

Decellularized ECM preserves biochemical and structural components of the native cellular niche and can modulate cell adhesion, proliferation, and differentiation [14, 15, 34]. Consistent with these properties, huaSMC-derived dECM increased p-AKT and reduced β-catenin signaling in PLA-overexpressing aortic VSMCs. AKT signaling is closely associated with cell survival and proliferation, whereas altered Wnt/β-catenin activity has been implicated in vascular remodeling and cellular senescence [33, 35]. Thus, modulation of these pathways may contribute to the partial rescue observed in our study. However, because the specific active components of the dECM and the causal roles of AKT and β-catenin were not directly tested, these findings should be interpreted as associations rather than definitive mechanisms.

Limitations

Several limitations should be acknowledged. First, this in vitro model does not reproduce the hemodynamic, immune, and metabolic environment of the intact vasculature. Second, only VSMCs from the umbilical artery and aorta were compared, limiting generalization to other vascular beds. Third, the specific dECM components responsible for the observed effects and the causal roles of AKT/β-catenin signaling were not determined. In addition, a GFP-ao + dECM control group was not included; therefore, the findings demonstrate that huaSMC-derived dECM partially mitigates PLA-associated phenotypes but do not establish a PLA-specific effect of dECM. Further studies incorporating appropriate dECM controls, molecular perturbation, ECM profiling, and in vivo validation are warranted.

Conclusion

In conclusion, PLA induced common senescence-associated abnormalities in VSMCs from both arterial origins, whereas downstream molecular and ECM responses differed between umbilical and aortic VSMCs. HuaSMC-derived dECM partially attenuated PLA-associated dysfunction in aortic VSMCs and was accompanied by modulation of AKT/β-catenin signaling. These findings demonstrate arterial origin-dependent heterogeneity in VSMC responses to nuclear envelope stress and support further investigation of ECM-mediated modulation of vascular cell senescence.

Acknowledgements

The authors are grateful to all laboratory members for insightful discussions and feedback. We would like to thank Professor Zhang Weiyi (Department of Obstetrics and Gynecology, Peking University Shenzhen Hospital) for providing the human aortic smooth muscle cells (huaSMCs) used in this study. We would like to thank Editage (www.editage.cn) for English language editing. This work was supported by the Shenzhen Science and Technology Innovation Program (grant number JCYJ20220531094006013) and Guangdong Basic and Applied Basic Research Foundation (grant number 2023A1515012394). Professional editing service costs were covered by these grants.

Disclosure of conflict of interest

None.

Address correspondence to: Dr. Yannv Qu, Geriatrics Department, Peking University Shenzhen Hospital, Shenzhen Peking University-The Hong Kong University of Science and Technology Medical Center, 1120 Lianhua Road, Futian District, Shenzhen 518036, Guangdong, China. Tel: +86-0755-83923333; E-mail: nacyququ@163.com

References

[1] Ragnauth CD, Warren DT, Liu Y, McNair R, Tajsic T, Figg N, Shroff R, Skepper J and Shanahan CM. Prelamin A acts to accelerate smooth muscle cell senescence and is a novel biomarker of human vascular aging. Circulation 2010; 121: 2200-2210.

[2] Liu Y, Drozdov I, Shroff R, Beltran LE and Shanahan CM. Prelamin A accelerates vascular calcification via activation of the DNA damage response and senescence-associated secretory phenotype in vascular smooth muscle cells. Circ Res 2013; 112: e99-e109.

[3] Warren DT, Tajsic T, Porter LJ, Minaisah RM, Cobb A, Jacob A, Rajgor D, Zhang QP and Shanahan CM. Nesprin-2-dependent ERK1/2 compartmentalisation regulates the DNA damage response in vascular smooth muscle cell ageing. Cell Death Differ 2015; 22: 1540-50.

[4] Uryga AK, Grootaert MOJ, Garrido AM, Oc S, Foote K, Chappell J, Finigan A, Rossiello F,

d'Adda di Fagagna F, Aravani D, Jorgensen HF and Bennett MR. Telomere damage promotes vascular smooth muscle cell senescence and immune cell recruitment after vessel injury. Commun Biol 2021; 4: 611.
[5] Zha Y, Zhuang W, Yang Y, Zhou Y, Li H and Liang J. Senescence in vascular smooth muscle cells and atherosclerosis. Front Cardiovasc Med 2022; 9: 910580.
[6] Worman HJ and Michaelis S. Permanently farnesylated prelamin A, progeria, and atherosclerosis. Circulation 2018; 138: 283-286.
[7] Hu Y, Cai Z and He B. Smooth muscle heterogeneity and plasticity in health and aortic aneurysmal disease. Int J Mol Sci 2023; 24: 11701.
[8] Muhl L, Mocci G, Pietilä R, Liu J, He L, Genové G, Leptidis S, Gustafsson S, Buyandelger B, Raschperger E, Hansson EM, Björkegren JLM, Vanlandewijck M, Lendahl U and Betsholtz C. A single-cell transcriptomic inventory of murine smooth muscle cells. Dev Cell 2022; 57: 2426-2443, e6.
[9] Dobnikar L, Taylor AL, Chappell J, Oldach P, Harman JL, Oerton E, Dzierzak E, Bennett MR, Spivakov M and Jørgensen HF. Disease-relevant transcriptional signatures identified in individual smooth muscle cells from healthy mouse vessels. Nat Commun 2018; 9: 4567.
[10] Yu Q, Li W, Jin R, Yu S, Xie D, Zheng X, Zhong W, Cheng X, Hu S, Li M, Zheng Q, Li G and Song Z. PI3Kγ (Phosphoinositide 3-Kinase γ) regulates vascular smooth muscle cell phenotypic modulation and neointimal formation through CREB (Cyclic AMP-Response Element Binding Protein)/YAP (Yes-Associated Protein) signaling. Arterioscler Thromb Vasc Biol 2019; 39: e91-e105.
[11] Barallobre-Barreiro J, Loeys B, Mayr M, Rienks M, Verstraeten A and Kovacic JC. Extracellular matrix in vascular disease, part 2/4: JACC focus seminar. J Am Coll Cardiol 2020; 75: 2189-2203.
[12] Lin PK and Davis GE. Extracellular matrix remodeling in vascular disease: defining its regulators and pathological influence. Arterioscler Thromb Vasc Biol 2023; 43: 1599-1616.
[13] Fu Y, Zhou Y, Wang K, Li Z and Kong W. Extracellular matrix interactome in modulating vascular homeostasis and remodeling. Circ Res 2024; 134: 931-949.
[14] Barbulescu GI, Bojin FM, Ordodi VL, Goje ID, Barbulescu AS and Paunescu V. Decellularized extracellular matrix scaffolds for cardiovascular tissue engineering: current techniques and challenges. Int J Mol Sci 2022; 23: 13040.
[15] Isaeva EV, Beketov EE, Arguchinskaya NV, Ivanov SA, Shegay PV and Kaprin AD. Decellularized extracellular matrix for tissue engineering (Review). Sovrem Tekhnologii Med 2022; 14: 57-68.
[16] Qu YN, Zhang L, Wang T, Zhang HY, Yang ZJ, Yuan FF, Wang Y, Li SW, Jiang XX and Xie XH. Vitamin C treatment rescues prelamin A-induced premature senescence of subchondral bone mesenchymal stem cells. Stem Cells Int 2020; 2020: 3150716.
[17] Schneider CA, Rasband WS and Eliceiri KW. NIH image to ImageJ: 25 years of image analysis. Nat Methods 2012; 9: 671-5.
[18] Crapo PM, Gilbert TW and Badylak SF. An overview of tissue and whole organ decellularization processes. Biomaterials 2011; 32: 3233-43.
[19] Dobnikar L, Taylor AL, Chappell J, Oldach P, Harman JL, Oerton E, Dzierzak E, Bennett MR, Spivakov M and Jørgensen HF. Disease-relevant transcriptional signatures identified in individual smooth muscle cells from healthy mouse vessels. Nat Commun 2018; 9: 4567.
[20] Dobrzynska A, Gonzalo S, Shanahan C and Askjaer P. The nuclear lamina in health and disease. Nucleus 2016; 7: 233-48.
[21] Dechat T, Pfleghaar K, Sengupta K, Shimi T, Shumaker DK, Solimando L and Goldman RD. Nuclear lamins: major factors in the structural organization and function of the nucleus and chromatin. Genes Dev 2008; 22: 832-853.
[22] Janetzko J, Oeck S and Schramm A. The multifaceted roles of lamins in lung cancer and DNA damage response. Cancers (Basel) 2023; 15: 5501.
[23] You W, Hong Y, He H, Huang X, Tao W, Liang X, Zhang Y and Li X. TGF-β mediates aortic smooth muscle cell senescence in Marfan syndrome. Aging (Albany NY) 2019; 11: 3574-3584.
[24] Kim HJ, Ham SA, Kim MY, Hwang JS, Lee H, Kang ES, Yoo T, Woo IS, Yabe-Nishimura C, Paek KS, Kim JH and Seo HG. PPARδ coordinates angiotensin II-induced senescence in vascular smooth muscle cells through PTEN-mediated inhibition of superoxide generation. J Biol Chem 2011; 286: 44585-93.
[25] Rapisarda V, Borghesan M, Miguela V, Encheva V, Snijders AP, Lujambio A and O'Loghlen A. Integrin beta 3 regulates cellular senescence by activating the TGF-β pathway. Cell Rep 2017; 18: 2480-2493.
[26] Zhu W, Kim BC, Wang M, Huang J, Isak A, Bexiga NM, Monticone R, Ha T, Lakatta EG and An SS. TGFβ1 reinforces arterial aging in the vascular smooth muscle cell through a long-range regulation of the cytoskeletal stiffness. Sci Rep 2018; 8: 2668.
[27] Grootaert MOJ, Moulis M, Roth L, Martinet W, Vindis C, Bennett MR and De Meyer GRY. Vascular smooth muscle cell death, autophagy

and senescence in atherosclerosis. Cardiovasc Res 2018; 114: 622-634.
[28] Wang H, Wan X, Pilch PF, Ellisen LW, Fried SK and Liu L. An AMPK-dependent, non-canonical p53 pathway plays a key role in adipocyte metabolic reprogramming. Elife 2020; 9: e63665.
[29] Demidenko ZN, Korotchkina LG, Gudkov AV and Blagosklonny MV. Paradoxical suppression of cellular senescence by p53. Proc Natl Acad Sci U S A 2010; 107: 9660-4.
[30] Huang Y, Huang D, Weng J, Zhang S, Zhang Q, Mai Z and Gu W. Effect of reversine on cell cycle, apoptosis, and activation of hepatic stellate cells. Mol Cell Biochem 2016; 423: 9-20.
[31] Cui XJ, Lin X, Zhong JY, Li S, He JY, Ni YQ, Zhan JK and Liu YS. Adiponectin attenuates the premature senescence of vascular smooth muscle cells induced by high glucose through mTOR signaling pathway. Aging Med (Milton) 2020; 3: 178-187.
[32] Donninger H, Calvisi DF, Barnoud T, Clark J, Schmidt ML, Vos MD and Clark GJ. NORE1A is a Ras senescence effector that controls the apoptotic/senescent balance of p53 via HIPK2. J Cell Biol 2015; 208: 777-89.
[33] Cai Z, Gong Z, Li Z, Li L and Kong W. Vascular extracellular matrix remodeling and hypertension. Antioxid Redox Signal 2021; 34: 765-783.
[34] Zhang S, Guo Y, Lu Y, Liu F, Heng BC and Deng X. The considerations on selecting the appropriate decellularized ECM for specific regeneration demands. Mater Today Bio 2024; 29: 101301.
[35] Liu J, Xiao Q, Xiao J, Niu C, Li Y, Zhang X, Zhou Z, Shu G and Yin G. Wnt/β-catenin signalling: function, biological mechanisms, and therapeutic opportunities. Signal Transduct Target Ther 2022; 7: 3.